
Optimize Weight Rounding via Signed Gradient Descent for the Quantization of LLMs

Wenhua Cheng

Intel

wenhua.cheng@intel.com

Weiwei Zhang

Intel

weiwei1.zhang@intel.com

Haihao Shen

Intel

haihao.shen@intel.com

Yiyang Cai

Intel

yiyang.cai@intel.com

Xin He

Intel

xin3.he@intel.com

Kaokao Lv

Intel

kaokao.lv@intel.com

Yi Liu

Intel

yi4.liu@intel.com

Abstract

Large Language Models (LLMs) have demonstrated exceptional proficiency in language-related tasks. However, their deployment presents significant challenges due to their substantial memory and storage requirements. To address this challenge, weight-only quantization has emerged as a promising solution. Previous research has indicated that fine-tuning through up and down rounding can enhance performance. In this study, we introduce SignRound, a method that utilizes signed gradient descent (SignSGD) to optimize rounding values and weight clipping within just 200 steps, combining the strengths of both Quantization-Aware Training (QAT) and Post-Training Quantization (PTQ). SignRound achieves outstanding results compared to recent methods across 2 to 4 bits, while maintaining low tuning costs and without introducing any additional inference overhead. For instance, SignRound led to absolute average accuracy improvements ranging from 6.91% to 33.22% at 2 bits. Furthermore, it demonstrates robust generalization to various recent models and achieves near-lossless quantization in most scenarios at 4 bits. The source code is publicly available at <https://github.com/intel/auto-round>.

1 Introduction

Large language models (LLMs) have demonstrated remarkable proficiency in language-related tasks [OpenAI, 2022, Touvron et al., 2023a]. However, deploying LLMs poses significant challenges due to their extensive memory and storage requirements. Additionally, the computational demands of these models create obstacles for real-time applications. Thus, studying techniques such as quantization becomes crucial to enable the efficient deployment of LLMs. Quantization techniques can be broadly categorized into two main types: quantization-aware training (QAT) [Esser et al., 2019, Zhuang et al., 2021, Lee et al., 2021, Liu et al., 2023b] and post-training quantization (PTQ) [Nagel et al., 2019, Xiao et al., 2022, Frantar et al., 2022, Nagel et al., 2020].

QAT involves training the model with quantization in mind. During QAT, the model is trained using simulated lower-precision representations, allowing it to learn and adapt to the effects of quantization. This approach often results in better accuracy compared to PTQ. However, QAT does come with certain drawbacks, including increased training complexity, longer training times, and the need to

tune hyperparameters. The application of QAT to LLMs can be particularly costly, despite recent efforts [Hu et al., 2021, Dettmers et al., 2023] to improve the efficiency of fine-tuning LLMs.

On the other hand, PTQ directly quantizes the model without any simulated training or fine-tuning. While PTQ is a more straightforward approach, it is susceptible to significant accuracy drops. This underscores the importance of further advancements in PTQ methods to enhance their accuracy preservation capabilities.

Two types of tensors commonly undergo quantization: activations and weights. Weight-only quantization has recently gained traction for LLMs due to its advantageous tradeoff. Quantizing activations for LLMs can be complex [Wei et al., 2022b, Xiao et al., 2023, Bondarenko et al., 2023], making weight-only quantization a more practical and feasible option. Moreover, the main bottleneck in generating new tokens for LLMs often arises from memory bandwidth limitations [Kim et al., 2023a], emphasizing the relevance of weight-only quantization.

This study focuses on weight-only quantization. In quantizing weights, a critical step involves rounding, primarily achieved through rounding-to-nearest (RTN). RTN quantizes each weight independently by rounding it to the nearest integer. However, RTN overlooks the relationships between weights as well as between weights and activations. Nagel et al. [Nagel et al., 2020] explored the potential for an enhanced rounding strategy to improve accuracy. They approached the rounding task by formulating it as a quadratic unconstrained binary optimization problem and approximating the loss using a Taylor series expansion. However, relying solely on the second-order term may not yield accurate results, as rounding can significantly modify weights, making other order terms non-negligible.

We chose SignSGD as our optimization method to approach the optimal rounding solution within a limited number of steps, drawing inspiration from the well-defined boundaries of the solution space. This space is confined to ranges of $[-0.5, 0.5]$ for rounding and $[0, 1]$ for weight clip scales, offering several advantages for SignSGD. Firstly, the optimal value for up and down rounding typically resides in a large region rather than a single float, as only the threshold for altering the rounding value is significant. This eliminates the necessity for the gradient magnitude to converge precisely to a single point. Secondly, due to these confined boundaries, SignSGD allows efficient navigation of this space within a limited number of steps. In contrast, optimizers like Adam [Kingma and Ba, 2014] may struggle due to significant variations in gradient magnitude, making it challenging to converge to the optimal value within a restricted number of steps. Thirdly, SignSGD is inherently intuitive, facilitating easy adjustment of the step size (learning rate). For example, we employed the same optimizer hyperparameters across all experiments unless explicitly stated, consisting of 200 steps and a learning rate of $5e - 3$, with linear weight decay. This ensures that $200 * 0.005/2 = 0.5$ covers the range of $[-0.5, 0.5]$ for rounding and $[0.5, 1]$ for weight clipping, which works well in practice. Fourthly, SignSGD stands out for its lightweight nature compared to other optimizers, requiring less memory and computational resources. Figure 1 provides an overview of our method. Our contributions primarily lie in three aspects:

- We introduce a concise yet effective method for optimizing the weight only quantization, combining the strengths of both QAT and PTQ. Our approach leverages SignSGD to tune the rounding with the weight clip, without introducing any additional overhead during inference.
- Our empirical results demonstrate a notable or significant enhancement in performance compared to recent works across different quantization configurations, from 2-bit to 4-bit.
- We demonstrate that SignRound’s performance can be further enhanced by fine-tuning model-wise hyperparameters within a constrained space. Moreover, our method demonstrates strong generalization across various models and delivers nearly lossless results across the majority of scenarios using 4-bit quantization.

2 Related Work

Quantization Aware Training. QAT methods have gained widespread popularity in model compression, as they enable the fine-tuning process [Esser et al., 2019, Zhuang et al., 2021, Lee et al., 2021] [Zhuang et al., 2021], often leading to superior accuracy compared to the PTQ method,

Post-training Quantization (PTQ). PTQ methods simplify the quantization process without the needs of additional training. [Nagel et al., 2019, Liu et al., 2021, Frantar and Alistarh, 2022, Hassibi et al., 1993, Yao et al., 2021, Wang et al., 2019]. Given its low resource requirement, PTQ is particularly suitable for the quantization of Large Language Models (LLMs).

Large Language Models Quantization. Significant strides have been made in addressing the pressing need for quantizing large language models (LLMs). LLM.int8() [Dettmers et al., 2022] introduces a mixed-precision approach to preserve crucial channels in high precision. PEQA [Kim et al., 2024] presents a simple yet effective method that combines the benefits of parameter-efficient fine-tuning (PEFT) with quantized LLMs. AQLM [Mao et al., 2024] builds upon Additive Quantization, a classic algorithm from the Multi-Codebook Quantization family, adapting it to LLM quantization. ZeroQuantV2 [Yao et al., 2023] employs low-rank matrices to enhance model quality recovery. RPTQ [Yuan et al., 2023] addresses range differences between channels by rearranging and quantizing them in clusters. Other methods, such as SPIQ [Yvinec et al., 2023b], SmoothQuant [Xiao et al., 2022], and Outlier Suppression+ [Wei et al., 2023], utilize handcrafted equivalent transformations to mitigate quantization errors. LLM-QAT [Liu et al., 2023b] employs QAT to enhance performance.

Weight only quantization. Weight-only quantization reduces the memory footprint and bandwidth demands by quantizing only the weights while retaining activations in floating-point precision, offering a promising balance between accuracy and compression. GPTQ [Frantar et al., 2022] optimizes weights using the Optimal Brain Surgeon technique [Hassibi et al., 1993], achieving low-bit quantization on LLMs with minimal tuning overhead. AWQ [Lin et al., 2023] follows the equivalent transformation approach with additional tuning in a constrained space, sharing similar limitations with SmoothQuant [Xiao et al., 2022]. TEQ [Cheng et al., 2023] and Omniquant [Shao et al., 2023] both utilize a trainable equivalent transformation, while Omniquant employs extra weight clip tuning. HQQ [Badri and Shaji, 2023] accelerates quantization for large models by eliminating the need for calibration data, making the quantization process extremely fast. Some other works have incorporated optimization methods with extra inference overhead to improve quantization accuracy, such as dense-and-sparse decomposition techniques in SqueezeLLM [Kim et al., 2023a] and EasyQuant [Tang et al., 2024], as well as nonuniform quantization methods in NUPES [Yvinec et al., 2023a], QuIP# [Tseng et al., 2024], [Gong et al., 2024], AQLM [Mao et al., 2024], etc. Additionally, FineQuant [Kim et al., 2023b] introduces a straightforward heuristic weight quantization approach that adaptively determines quantization granularity. In this work, we focus on approaches that do not introduce overhead during inference.

Rounding Methods. Adaptive Rounding [Nagel et al., 2020] has already showcased the potential of an advanced rounding strategy to enhance accuracy [Li et al., 2021, Wei et al., 2022a]. They used the rounding task as a quadratic unconstrained binary optimization problem by approximating the task loss through a Taylor series expansion. However, considering only the second-order term may not yield accurate results. This is because the rounding value gets multiplied by a scaling coefficient during de-quantization, potentially introducing significant weight changes that make other order terms non-negligible. FlexRound [Lee et al., 2023] introduces a more flexible approach to rounding by incorporating element-wise division. However, it’s not easily scalable to apply to LLMs due to the needs of specialized hyperparameters for each specific model and task. Furthermore, Oscillation-free [Liu et al., 2023a] suggests that the introduction of learnable parameters might result in weight oscillation problems. AQuant [Li et al., 2022] introduced a dynamic approach where the border becomes a function dependent on the activation value to reduce the quantization error of activation.

Signed Gradient Descent. Signed gradient descent is not commonly utilized and is typically applied in specific scenarios, such as reducing communication costs. This is because signed gradient carries significantly less information compared to original gradient. Recent studies have shed light on the advantages of sign-based methods over gradient descent in certain conditions. Safaryan et al. [Safaryan and Richtárik, 2021] found that sign-based methods are preferable when the Hessian matrix is concentrated on its diagonal and the maximal eigenvalue is much larger than the average eigenvalue. Li et al. [Li et al., 2023a] investigated a variant of sign-based gradient descent that exhibits faster convergence. Additionally, Safaryan et al. [Safaryan and Richtárik, 2021] proposed a stochastic sign descent with momentum, which converges under the standard bounded variance assumption with the optimal asymptotic rate. These findings contribute to a better understanding of the potential benefits and applications of signed gradient descent methods.

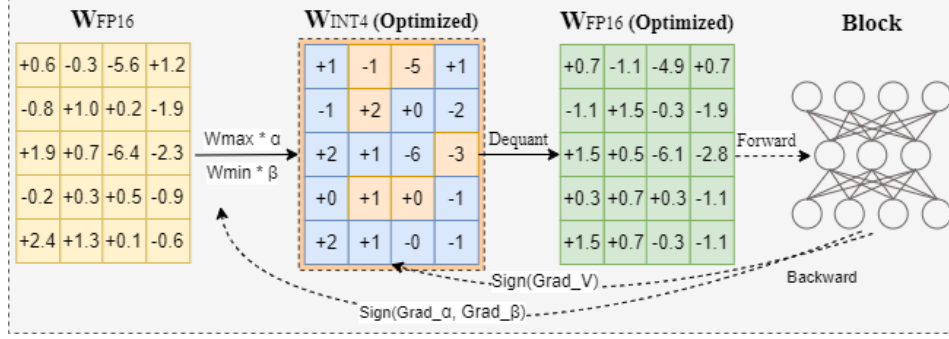


Figure 1: An illustration of SignRound. Unlike the direct rounding in RTN, SignRound performs signed gradient descent to fine-tune the up and down rounding through block-wise output reconstruction. After lightweight forward and backward steps, \mathbf{W}_{INT4} has been well optimized towards the minimal loss, therefore ready for the final inference deployment. Note that Quant and Dequant are two standard operations for quantization and de-quantization respectively.

3 Methodology

We begin with an overview of quantization before delving into the specifics of our approach. The following operations can be utilized to quantize and de-quantize the weights W :

$$\widetilde{W} = s * \text{clip}\left(\left\lfloor \frac{W}{s} + zp \right\rfloor, n, m\right), n, m \in \mathbb{N} \quad (1)$$

where the rounding operation $\lfloor \cdot \rfloor$ is typically performed using the RTN method. Although RTN is a concise approach, it quantizes each element independently, which results in the loss of the ability to model the correlation among different weights or activations. The s represents the quantization scale, which can be obtained using the following equation, and zp is the zero point.

$$s = \frac{\max(W) - \min(W)}{2^{\text{bit}} - 1} \quad (2)$$

In order to improve the efficacy of the rounding quantization operation, we build upon prior research [Nagel et al., 2020] by introducing a single trainable parameter V to adjust the rounding values.

$$\widetilde{W} = s * \text{clip}\left(\left\lfloor \frac{W}{s} + zp + V \right\rfloor, n, m\right), n, m \in \mathbb{N} \quad (3)$$

Additionally, following recent works [Lin et al., 2023, Shao et al., 2023], we introduce two additional trainable parameters, denoted as $\alpha \in [0, 1]$ and $\beta \in [0, 1]$, to fine-tune the scale of weight clipping. These parameters are incorporated into the equations as follows:

$$s = \frac{\max(W) * \alpha - \min(W) * \beta}{2^{\text{bit}} - 1} \quad (4)$$

These modifications enable a more adaptable quantization process. We utilize block-wise output reconstruction to train these parameters via optimizer, thus framing the optimization as follows.

$$\min_{\alpha, \beta, V} \|WX - \widetilde{W}X\|_F^2 \quad (5)$$

where X is the input of the block and $\|\cdot\|_F$ denotes the Frobenius norm.

Our method distinguishes itself primarily by leveraging SignSGD, with the motivation thoroughly outlined in Section Introduction 1. Figure 1 provides an illustration of our approach. And the pseudocode 1 presents more details of SignRound.

Algorithm 1 SignRound

Input: Calibration Data \mathcal{D} , learning rate lr , total steps T , Model M , block module m_w with weights w , batch size bs

Output: $best_V, best_alpha, best_beta$

```
1:  $V \leftarrow 0, \alpha \leftarrow 1.0, \beta \leftarrow 1.0, best\_l \leftarrow maximum$ 
2: for  $i \leftarrow 0$  to  $T$  do
3:    $d \leftarrow draw\ bs\ samples\ from\ previous\ quantized\ block$ 
4:    $x \leftarrow M(d)_m$  ▷ get the inputs of m
5:    $y_f \leftarrow m_w(x)$  ▷ get the output of original module
6:    $\tilde{w} \leftarrow qdq(w, \alpha, \beta, V)$  ▷ quantize and dequantize w via Eq.3
7:    $y_q \leftarrow m_{\tilde{w}}(x)$  ▷ get the output of quantized module
8:    $loss \leftarrow mse(y_q, y_f)$  ▷ get the loss via Eq.5
9:    $loss.backward()$ 
10:  if  $loss < best\_l$  then
11:     $best\_V, best\_alpha, best\_beta \leftarrow V, \alpha, \beta$ 
12:     $best\_l \leftarrow loss$ 
13:  end if
14:  update  $\alpha, \beta$  and  $V$  via SignSGD optimizer
15: end for
```

4 Experiments

In this section, we conduct a comprehensive evaluation of SignRound from various perspectives. Initially, we offer a concise overview of the LLM architectures and tasks encompassed in our assessment. Next, we delve into a detailed comparison between our method and several existing approaches, highlighting the unique advantages of SignRound. Furthermore, we conduct ablation studies to strengthen the efficacy of our choices and explore the sensitivity of hyperparameters. Lastly, we assess the generation ability of our method across various recent models. The tuning cost comparisons are present in Appendix A.

4.1 Experimental Settings

Evaluation and tasks. We evaluate multiple language tasks to accommodate the task-agnostic setting. Specifically, we present the average accuracy results for 11 zero shot tasks, including HellaSwag [Zellers et al., 2019], WinoGrande [Sakaguchi et al., 2021], PIQA [Bisk et al., 2020], LAMBADA [Paperno et al., 2016], TruthfulQA [Lin et al., 2021], OpenBookQA [Mihaylov et al., 2018], BoolQ [Clark et al., 2019], RTE [Dagan et al., 2010], ARC-Easy, ARC-Challenge [Clark et al., 2018] and MMLU [Hendrycks et al., 2020]. We use lm-eval-harness[Gao et al., 2023] for all the above tasks. Furthermore, we complement our evaluation with perplexity (ppl) analysis on Wikitext2 [Merity et al., 2016] PTB [Marcus et al., 1993] and C4 [Raffel et al., 2020], by following the source code ¹ of GPTQ and Wikitext2 [Merity et al., 2016] using lm-eval-harness[Gao et al., 2023]. However, We argue that perplexity is notably influenced by outliers, as illustrated in Table 14 for different algorithms. This susceptibility likely arises from the mathematical expression $PPL(X) = \exp\left(-\frac{1}{t} \sum_{i=1}^t \log p_{\theta}(x_i | x_{<i})\right)$, where assigning a low probability to even one token can significantly inflate the perplexity score. Consequently, we prioritize the accuracy of the 11 tasks mentioned above as the primary metric, with perplexity data serving as a supplementary reference.

Quantization Configurations. In accordance with GPTQ [Frantar et al., 2022], our focus lies specifically on weight-only quantization, targeting the linear layers within transformer blocks. Layers such as the embedding layer and typically the last linear layer like 'lm-head' are excluded from the quantization process. Our evaluation primarily centers on W4, W4G128, and W3G128 configurations, where W4 indicates quantizing weights with 4 bits and G represents finer-grained grouping as described in [Park et al., 2022, Frantar et al., 2022]. We adopt asymmetric quantization for these configurations. For calibration and to mitigate overfitting on the WikeText and C4 datasets, we

¹<https://github.com/IST-DASLab/gptq>

randomly select 512 samples with the same seed from the readily available pile-10k dataset ², which comprises the first 10k samples from pile [Gao et al., 2020]. We used a sequence length of 2048 for calibration, while for other methods, we adhere to their official settings

Large Language Models. We compare different algorithms on LLaMA-V1 [Touvron et al., 2023a], LLaMA-V2 [Touvron et al., 2023b] and Mistral-7B-v0.1 [Jiang et al., 2023] as they are commonly used. We cover a wide range of LLM parameters, ranging from 7B to 70B, to ensure comprehensive coverage and analysis.

Table 1: Average accuracies(\uparrow) across 11 tasks, detailed in Section 4.1, of LLaMA and Mistral models at W2-W4. Our* denotes the highest accuracy achieved among the 8 hyperparameter choices, detailed in Section 4.2, whereas for the 70B model, we only tested a few options.

Config	Method	Mistral-7B	V2-7B	V2-13B	V2-70B	Config	Method	Mistral-7B	V2-7B	V2-13B	V2-70B
	FP16	63.30	57.98	61.42	66.12		FP16	63.30	57.98	61.42	66.12
W4G-1	RTN	58.84	55.49	60.46	65.22	W3G128	RTN	58.20	53.81	58.57	64.08
	HQQ	58.40	46.05	46.82	57.47		HQQ	59.33	54.31	58.10	64.80
	Omni	60.52	56.62	60.31	65.80		Omni	58.53	54.72	59.18	65.12
	GPTQ	61.37	56.76	59.79	65.75		GPTQ	59.91	54.14	59.58	65.08
	AWQ	61.36	57.25	60.58	66.28		AWQ	59.96	55.21	58.86	65.12
	Ours	62.33	57.48	61.20	66.27		Ours	60.43	56.68	59.44	65.31
	Ours*	62.64	57.52	61.23	66.27		Ours*	60.96	56.68	59.78	65.59
W4G128	RTN	62.36	56.92	60.65	65.87	W2G128	RTN	30.52	29.94	33.51	38.14
	HQQ	62.75	57.41	60.65	66.06		HQQ	31.41	29.87	35.28	37.42
	Omni	62.18	57.30	60.51	66.02		Omni	32.17	40.74	46.55	51.31
	GPTQ	62.32	56.85	61.00	66.22		GPTQ	39.61	35.37	42.46	28.47
	AWQ	62.16	57.35	60.91	66.23		AWQ	30.06	30.10	32.16	32.23
	Ours	62.62	57.57	60.85	66.39		Ours	52.71	48.64	53.46	61.69
	Ours*	62.87	57.97	60.90	66.41		Ours*	53.01	50.34	54.16	61.77

SignRound Hyper-parameters. Unless explicated stated, the tuning process involved adjusting each block for 200 steps, with the learning rate(lr) as 1/steps, i.e. $5e - 3$, a batch size of 8 and linear lr decay. Additionally, we employed automatic mixed precision (AMP) to accelerate the tuning.

4.2 Comparing With Recent Methods

In this section, we compare our methods with those that have already demonstrated remarkable results and impose no additional overhead on our tested models in weight-only quantization for LLMs, including GPTQ [Frantar et al., 2022], AWQ [Lin et al., 2023], HQQ [Badri and Shaji, 2023], Omniquant, [Shao et al., 2023] with a naive method RTN.

To ensure fair comparison as much as possible, we have enabled act-order and true-sequential in GPTQ, and also activated static_group in scenarios where $group_size \neq -1$. The notation GPTQ⁺ indicates that we adjusted the random seed or data pre-processing to address issues related to the non-positive definite Hessian matrix or other issues. For Omniquant[Shao et al., 2023], we adhere to the official settings, which include running for 20 epochs including W2G128 for saving time and disabling 'let'. We conducted calibration tests using sample sizes of 512 and 128, as well as a sample size of 512 with a batch size of 4. Our findings show that using a sample size of 512 typically results in comparable or slight higher performance for models $\leq 13B$. Therefore, we present the results based on the sample size of 512. For 70B models, due to the NAN loss issue and to reduce the tuning cost of Omniquant, we adopted 128 samples for calibration.

We present the summary results of Mistral-7B and LLaMA V2 in Table 1, detailed results of W4G-1 in Table 2. Additional detailed results are provided in Appendix C due to space constraints. In summary, our approach demonstrated superior performance compared to GPTQ [Frantar et al., 2022], achieving scores of 30/32, AWQ [Lin et al., 2023] with 27/32, HQQ [Badri and Shaji, 2023] with 15/16, and OmniQuant [Shao et al., 2023] with a score of 29/32 across llama1/llama2/mistral-7b on various quantization settings, including W4G-1, W4G128, W3G128, and W2G128. These evaluations were based on the average accuracies of 11 zero-shot tasks.

²<https://huggingface.co/datasets/NeelNanda/pile-10k>

Table 2: Detrailed accuracies(\uparrow) across 11 tasks(0-shot) of LLaMA and Mistral models at W4G-1. Our* denotes the highest accuracy achieved among the 8 hyperparameter choices, whereas for the 70B model, we only tested a few options, detailed in 4.2. Appendix C provides more detailed data.

Model	Method	Mmlu	Lamb.	Hella.	Wino.	Piqa	Truth.	Open.	Boolq	RTE	ARC-e	ARC-c.	Avg.
Mistral-7B	FP16	61.35	75.68	61.27	74.03	80.79	28.03	32.80	83.67	67.51	80.81	50.34	63.30
	RTN	55.92	66.10	59.01	71.35	80.14	24.85	29.00	79.17	57.76	77.95	45.99	58.84
	GPTQ	58.22	73.45	59.47	74.03	80.20	26.93	31.00	81.50	64.98	78.24	47.01	61.37
	AWQ	57.20	71.45	59.21	73.64	79.43	25.34	30.40	82.69	68.95	79.25	47.44	61.36
	HQQ	52.65	66.58	59.09	70.56	79.60	23.13	27.80	80.03	59.57	77.02	46.33	58.40
	Omni	57.52	70.00	60.27	72.93	79.87	23.99	30.80	81.53	63.90	78.54	46.42	60.52
	Ours	59.52	73.76	60.75	73.32	80.09	27.17	33.00	82.02	66.07	80.47	49.49	62.33
	Ours*	60.00	73.30	60.57	74.35	80.09	27.91	32.20	83.52	67.51	79.92	49.66	62.64
V2-7B	FP16	42.69	73.90	57.15	68.90	78.07	25.21	31.40	77.74	62.82	76.35	43.52	57.98
	RTN	36.87	67.96	55.63	68.51	76.82	26.19	30.60	73.64	58.84	74.07	41.30	55.49
	GPTQ	39.66	71.92	55.89	68.03	77.58	25.09	30.20	76.67	62.09	75.55	41.72	56.76
	AWQ	40.24	71.20	56.26	69.61	76.93	26.07	32.60	77.31	63.18	75.00	41.30	57.25
	HQQ	28.94	43.96	48.43	59.43	71.82	23.62	24.80	52.11	53.79	64.90	34.73	46.05
	Omni	39.82	71.45	55.76	67.56	76.88	25.09	30.80	76.15	64.98	74.12	40.19	56.62
	Ours	39.97	71.63	56.52	68.43	77.91	25.70	31.60	76.18	65.70	76.01	42.58	57.48
	Ours*	40.85	72.75	56.01	67.88	77.86	25.34	31.80	76.39	66.43	75.88	41.55	57.52
V2-13B	FP16	52.86	76.77	60.04	72.14	79.05	25.95	35.20	80.55	65.34	79.38	48.38	61.42
	RTN	50.37	74.35	59.12	71.98	79.00	24.85	33.00	81.77	64.98	79.08	46.59	60.46
	GPTQ	51.14	75.37	59.14	72.06	78.02	25.34	32.20	80.46	62.09	77.36	44.54	59.79
	AWQ	51.16	75.98	59.51	70.80	78.40	25.21	34.60	78.26	66.79	79.12	46.59	60.58
	HQQ	35.92	49.54	46.27	58.01	72.47	23.99	19.80	61.77	51.26	62.84	33.19	46.82
	Omni	51.01	75.45	59.48	71.74	78.94	24.60	33.20	77.37	66.07	78.75	46.76	60.31
	Ours	52.30	75.96	59.79	72.30	78.84	25.58	34.00	80.15	66.79	79.38	48.12	61.20
	Ours*	52.29	76.15	59.73	71.90	78.51	25.21	34.40	80.24	67.51	79.34	48.21	61.23
V2-70B	FP16	66.23	79.64	64.77	77.98	82.15	30.60	37.20	83.70	67.87	82.70	54.44	66.12
	RTN	63.85	77.62	63.38	76.72	81.50	28.89	37.80	83.39	68.23	81.99	54.10	65.22
	GPTQ	64.81	79.27	63.86	76.87	81.61	31.46	36.40	82.23	70.04	82.53	54.18	65.75
	AWQ	65.08	78.77	64.14	77.11	81.45	30.48	37.20	83.64	72.92	82.49	55.80	66.28
	HQQ	56.45	66.74	53.67	73.32	76.50	25.58	33.40	67.95	61.73	72.90	43.94	57.47
	Omni	64.40	79.20	63.91	76.95	81.94	31.70	37.60	82.35	69.31	82.24	54.18	65.80
	Ours	65.43	79.55	64.47	78.06	82.10	30.60	36.40	83.91	71.12	82.53	54.78	66.27

It’s worthy to noting that, as the bits going down, the advantages of Signround becomes more notable. For example, at W2G128, SignRound could yield absolute average accuracy improvements ranging from 6.91% to 33.22%.

Moreover, we can enhance the performance by optimizing the model’s hyperparameters from a selection of eight choices, denoted as ours*. These include steps (200, 1000), weight clip lr (1.0/steps, 2.0/steps), and the option to either enable or disable quanted inputs which means utilizing the output from the previous quanted block or the previous original block.

4.3 Comparing With Rounding Methods

In this section, we conduct a comparative analysis between SignRound, FlexRound[Lee et al., 2023], and AdaRound[Nagel et al., 2020]. Notably, there is no formal official implementation available for FlexRound and AdaRound for LLMs. Hence, we reference the code³ for further details. However, it’s important to highlight that due to the lack of AMP support and other optimizations, the implementation is notably slow, especially when adhering to the official settings, which involve tuning 5000 steps, as presented in Table 9. Hence, our comparison is limited to models of size 13B or smaller. We set the learning rate to 2e-4 for LLaMA-2-7b and Mistral-7B, and 1e-4 for LLaMA-13-7b to align with the official settings as closely as possible.

³https://openreview.net/forum?id=-tYCaPOpHY_

Table 3: Comparing with other rounding methods, the average accuracies (\uparrow) across 11 tasks (detailed in 4.1) for Mistral and LLaMA models at W4G-1 and W2G128.

Model	Method	Iter.	Mistral-7B	V2-7B	V2-13B
W4G-1	Flex	200	58.93	56.10	60.06
		1000	60.62	56.98	60.29
		5000	60.94	57.49	-
	Ada	200	58.30	55.06	59.86
		1000	58.38	55.05	59.92
	Ours	200	62.33	57.48	61.20
200*		62.64	57.52	61.23	
W2G128	Flex	200	30.10	30.01	30.66
		1000	30.16	31.26	32.29
	Ada	200	30.74	30.21	30.36
		1000	30.84	30.30	30.02
	Ours	200	52.71	48.64	53.46
		200*	53.01	50.34	54.16

4.4 Ablation Study

SignSGD versus Adam. To validate the effectiveness of SignSGD, Table 4 compares it with the Adam optimizer. SignSGD employs a fixed learning rate of $5e-3$ throughout all experiments, comprising 200 steps, with linear weight decay. For Adam, we explored initial learning rates ranging from $2.5e-3$ to $2e-2$. We choose to quantize models of 13B or less with W4G-1 due to the experiment’s cost. SignSGD demonstrated a distinct advantage in average accuracy metrics across 11 tasks, which demonstrate the unique advantage of signed gradient descent in this scenario.

Table 4: Adam optimizer with various learning rates vs. SignSGD optimizer. The average accuracies(\uparrow) across 11 tasks (detailed in 4.1) for Mistral and LLaMA models at W4G-1 and W2G128.

Config	Model	2.5e-3	5e-3	7.5e-3	1e-2	1.25e-2	1.5e-2	1.75e-2	2e-2	SignSGD
W4G-1	Mistral-7B	61.82	61.16	61.30	60.69	60.80	61.07	61.53	61.23	62.33
	V2-7B	56.79	57.45	57.09	57.28	56.88	57.24	57.40	57.10	57.48
	V2-13B	60.58	60.73	60.76	60.86	61.02	60.79	61.06	60.85	61.20
W2G128	Mistral-7B	37.12	40.37	41.11	42.02	42.86	43.55	43.44	42.44	52.71
	V2-7B	42.26	44.64	45.08	45.04	45.15	43.13	38.71	35.73	48.64
	V2-13B	47.81	50.01	49.55	50.80	48.67	51.94	38.28	34.67	53.46

Round and Weight clip tuning To validate the contributions of rounding tuning and weight clip tuning, we conducted ablation studies on three models with two quantization configurations. As shown in Table 5, each component provides benefits over RTN, with rounding tuning offering greater advantages. However, when combined, weight clip tuning can sometimes result in lower accuracy in some cases at W2G128.

Table 5: Ablation study of Round tuning and weight clip tuning. The average accuracies(\uparrow) across 11 tasks(detailed in 4.1) for Mistral and LLaMA models at W4G-1 and W2G128.

Config	Mistral-7B	V2-7B	V2-13B	Mistral-7B	V2-7B	V2-13B
	W4G-1			W2G128		
RTN	58.84	55.49	60.46	30.52	29.94	33.51
Weight clip only	61.10	57.41	60.10	46.60	40.53	49.77
Rounding only	61.62	56.74	60.64	52.32	49.14	54.41
Default	62.33	57.48	61.20	52.71	48.64	53.46

Hyperparameters sensitivity To validate the sensitivity of hyperparameters in SignRound, we conducted ablation studies on sequence length for calibration, number of samples for calibration, tuning batch size, tuning steps, and tuning learning rate. The results are presented in Table 6. Overall, our default hyperparameters achieved balanced results.

Table 6: Ablation study of of hyperparameter sensitivity. The average accuracies(\uparrow) across 11 tasks(detailed in 4.1) for LLaMA models at W4G-1.

Model	SeqLen_512	Samples_128	Batch_4	Iters_100	LR_1e-2	Default
Mistral-7B	60.32	61.82	61.78	61.06	61.27	62.33
V2-7B	57.91	56.41	57.21	57.10	55.89	57.48
V2-13B	60.88	60.87	61.21	60.80	61.03	61.20

4.5 Generalization to other models

To assess the generalization of our method on LLMs, we evaluate SignRound on various mainstream LLMs like Gemma [Team et al., 2024], Phi [Li et al., 2023b], Mistral [Jiang et al., 2023], Mixtral [Jiang et al., 2024] and Llama3 [Touvron et al., 2024]. Table 7 demonstrated that all int4 models met the requirement of maintaining accuracy drop within 1% of the FP16 or BF16 accuracy by employing 1000 tuning steps and model wise hype-parameters among 4 choices detailed in section 4.1. Additionally, one-third of the models exhibited a slight improvement in accuracy compared to the baseline. Please note that the generalization experiments utilize an updated version (0.4.0+) of lm-eval-harness [Gao et al., 2023] and real quantized model, which may result in minor discrepancies compared to other benchmark data.

Table 7: Accuracies(\uparrow) across 11 tasks(0-shot) with 1000 steps for LLMs at W4G128

Model	Method	Mmlu	Lamb.	Hella.	Wino.	Piqa	Truth.	Open.	Boolq	RTE	ARC-e	ARC-c.	Avg.	Vari.	%
gemma-7b	FP16	61.62	67.51	60.47	73.24	79.43	30.97	33.20	82.78	65.34	81.78	49.91	62.39	-	-
	Ours	61.47	72.04	59.03	75.14	79.49	30.11	34.00	82.69	70.76	79.59	49.40	63.07	1.09%	-
gemma-7b-it	FP16	50.29	60.35	56.20	67.96	77.09	30.48	37.40	81.38	78.70	75.25	47.27	60.22	-	-
	Ours	49.93	62.86	55.64	67.88	77.31	30.35	37.00	81.44	78.70	75.08	45.73	60.17	-0.08%	-
Llama-2-7b-chat	FP16	46.40	71.05	57.80	66.38	76.39	30.23	33.40	79.76	69.68	73.82	44.20	59.01	-	-
	Ours	45.45	70.37	57.06	66.14	76.33	30.35	32.60	80.64	72.92	73.36	43.52	58.97	-0.07%	-
Llama-3-8B-Instruct	BF16	63.86	71.82	57.69	71.43	78.67	36.23	34.00	82.97	67.51	81.52	52.99	63.52	-	-
	Ours	63.06	72.00	56.99	72.38	77.97	35.37	33.00	83.09	68.59	80.89	51.02	63.12	-0.63%	-
Mistral-7B	BF16	59.61	75.61	61.28	74.43	80.79	28.03	32.80	83.73	66.43	80.85	50.09	63.06	-	-
	Ours	58.80	75.51	60.79	74.51	80.14	28.89	33.00	82.78	69.68	80.60	49.15	63.08	0.03%	-
Mixtral-8x7B	BF16	68.02	78.27	64.90	76.48	82.48	34.27	35.40	85.23	70.76	84.30	56.66	66.98	-	-
	Ours	66.93	78.25	64.59	75.14	82.10	32.19	35.60	84.74	69.31	84.30	56.48	66.33	-0.97%	-
Mixtral-8x7B-Instruct	BF16	68.85	77.18	67.67	76.87	83.51	49.69	36.80	88.50	71.84	86.99	62.20	70.00	-	-
	Ours	68.24	77.90	67.45	77.19	83.35	48.84	37.20	87.83	70.04	87.12	62.29	69.77	-0.33%	-
Phi-3-mini-4k-instruct	FP16	68.20	68.14	60.64	73.88	80.14	39.53	38.40	86.24	78.34	83.42	55.63	66.93	-	-
	Ours	67.28	66.78	59.69	73.17	79.43	37.58	39.00	85.81	77.98	83.33	56.48	66.33	-0.90%	-

5 Conclusions and Limitations.

In this paper, we introduce SignRound, an efficient and succinct approach to optimizing weight rounding in quantization tasks. SignRound leverages signed gradient descent for lightweight block-wise tuning, resulting in significant quantization enhancements with minimal iteration steps. Our extensive experiments demonstrate that SignRound outperforms other quantization methods across various models and evaluation metrics while maintaining fixed hyperparameter configurations and similar fine-tuning time costs. Additionally, SignRound offers increased flexibility in quantizing specific large language models, achieving enhanced quantization performance with appropriately tuned hyperparameters.

Despite these significant advantages, we still observed a noticeable gap in the accuracy performance of ultra-low bit quantization compared to the original model, such as 2-bit quantization. This challenge could potentially be addressed by exploring non-uniform quantization and mixed-precision quantization, which we leave it as the future work.

References

- Hicham Badri and Appu Shaji. Half-quadratic quantization of large machine learning models, November 2023. URL https://mobiusml.github.io/hqq_blog/.
- Yonatan Bisk, Rowan Zellers, Jianfeng Gao, Yejin Choi, et al. Piqa: Reasoning about physical commonsense in natural language. In *Proceedings of the AAAI conference on artificial intelligence*, volume 34, pages 7432–7439, 2020.
- Yelysei Bondarenko, Markus Nagel, and Tijmen Blankevoort. Quantizable transformers: Removing outliers by helping attention heads do nothing. *arXiv preprint arXiv:2306.12929*, 2023.
- Wenhua Cheng, Yiyang Cai, Kaokao Lv, and Haihao Shen. Teq: Trainable equivalent transformation for quantization of llms. *arXiv preprint arXiv:2310.10944*, 2023.
- Christopher Clark, Kenton Lee, Ming-Wei Chang, Tom Kwiatkowski, Michael Collins, and Kristina Toutanova. Boolq: Exploring the surprising difficulty of natural yes/no questions. *arXiv preprint arXiv:1905.10044*, 2019.
- Peter Clark, Isaac Cowhey, Oren Etzioni, Tushar Khot, Ashish Sabharwal, Carissa Schoenick, and Oyvind Tafjord. Think you have solved question answering? try arc, the ai2 reasoning challenge. *arXiv preprint arXiv:1803.05457*, 2018.
- Ido Dagan, Bill Dolan, Bernardo Magnini, and Dan Roth. Recognizing textual entailment: Rational, evaluation and approaches—erratum. *Natural Language Engineering*, 16(1):105–105, 2010.
- Tim Dettmers, Mike Lewis, Younes Belkada, and Luke Zettlemoyer. Llm.int8(): 8-bit matrix multiplication for transformers at scale. *arXiv preprint arXiv:2208.07339*, 2022.
- Tim Dettmers, Artidoro Pagnoni, Ari Holtzman, and Luke Zettlemoyer. Qlora: Efficient finetuning of quantized llms. *arXiv preprint arXiv:2305.14314*, 2023.
- Steven K Esser, Jeffrey L McKinstry, Deepika Bablani, Rathinakumar Appuswamy, and Dharmendra S Modha. Learned step size quantization. *arXiv preprint arXiv:1902.08153*, 2019.
- Elias Frantar and Dan Alistarh. Optimal brain compression: A framework for accurate post-training quantization and pruning. *arXiv preprint arXiv:2208.11580*, 2022.
- Elias Frantar, Saleh Ashkboos, Torsten Hoefler, and Dan Alistarh. Gptq: Accurate post-training quantization for generative pre-trained transformers. *arXiv preprint arXiv:2210.17323*, 2022.
- Leo Gao, Stella Biderman, Sid Black, Laurence Golding, Travis Hoppe, Charles Foster, Jason Phang, Horace He, Anish Thite, Noa Nabeshima, et al. The pile: An 800gb dataset of diverse text for language modeling. *arXiv preprint arXiv:2101.00027*, 2020.
- Leo Gao, Jonathan Tow, Baber Abbasi, Stella Biderman, Sid Black, Anthony DiPofi, Charles Foster, Laurence Golding, Jeffrey Hsu, Alain Le Noac’h, Haonan Li, Kyle McDonell, Niklas Muennighoff, Chris Ociepa, Jason Phang, Laria Reynolds, Hailey Schoelkopf, Aviya Skowron, Lintang Sutawika, Eric Tang, Anish Thite, Ben Wang, Kevin Wang, and Andy Zou. A framework for few-shot language model evaluation, 12 2023. URL <https://zenodo.org/records/10256836>.
- Zhuocheng Gong, Jiahao Liu, Jingang Wang, Xunliang Cai, Dongyan Zhao, and Rui Yan. What makes quantization for large language model hard? an empirical study from the lens of perturbation. In *Proceedings of the AAAI Conference on Artificial Intelligence*, volume 38, pages 18082–18089, 2024.
- Babak Hassibi, David G Stork, and Gregory J Wolff. Optimal brain surgeon and general network pruning. In *IEEE international conference on neural networks*, pages 293–299. IEEE, 1993.
- Dan Hendrycks, Collin Burns, Steven Basart, Andy Zou, Mantas Mazeika, Dawn Song, and Jacob Steinhardt. Measuring massive multitask language understanding. *arXiv preprint arXiv:2009.03300*, 2020.

- Edward J Hu, Yelong Shen, Phillip Wallis, Zeyuan Allen-Zhu, Yuanzhi Li, Shean Wang, Lu Wang, and Weizhu Chen. Lora: Low-rank adaptation of large language models. *arXiv preprint arXiv:2106.09685*, 2021.
- Albert Q Jiang, Alexandre Sablayrolles, Arthur Mensch, Chris Bamford, Devendra Singh Chaplot, Diego de las Casas, Florian Bressand, Gianna Lengyel, Guillaume Lample, Lucile Saulnier, et al. Mistral 7b. *arXiv preprint arXiv:2310.06825*, 2023.
- Albert Q Jiang, Alexandre Sablayrolles, Antoine Roux, Arthur Mensch, Blanche Savary, Chris Bamford, Devendra Singh Chaplot, Diego de las Casas, Emma Bou Hanna, Florian Bressand, et al. Mixtral of experts. *arXiv preprint arXiv:2401.04088*, 2024.
- Jeonghoon Kim, Jung Hyun Lee, Sungdong Kim, Joonsuk Park, Kang Min Yoo, Se Jung Kwon, and Dongsoo Lee. Memory-efficient fine-tuning of compressed large language models via sub-4-bit integer quantization. *Advances in Neural Information Processing Systems*, 36, 2024.
- Sehoon Kim, Coleman Hooper, Amir Gholami, Zhen Dong, Xiuyu Li, Sheng Shen, Michael W Mahoney, and Kurt Keutzer. Squeezellm: Dense-and-sparse quantization. *arXiv preprint arXiv:2306.07629*, 2023a.
- Young Jin Kim, Rawn Henry, Raffy Fahim, and Hany Hassan Awadalla. Finequant: Unlocking efficiency with fine-grained weight-only quantization for llms. *arXiv preprint arXiv:2308.09723*, 2023b.
- Diederik P Kingma and Jimmy Ba. Adam: A method for stochastic optimization. *arXiv preprint arXiv:1412.6980*, 2014.
- Jung Hyun Lee, Jihun Yun, Sung Ju Hwang, and Eunho Yang. Cluster-promoting quantization with bit-drop for minimizing network quantization loss. In *Proceedings of the IEEE/CVF International Conference on Computer Vision*, pages 5370–5379, 2021.
- Jung Hyun Lee, Jeonghoon Kim, Se Jung Kwon, and Dongsoo Lee. Flexround: Learnable rounding based on element-wise division for post-training quantization. *arXiv preprint arXiv:2306.00317*, 2023.
- Xiuxian Li, Kuo-Yi Lin, Li Li, Yiguang Hong, and Jie Chen. On faster convergence of scaled sign gradient descent. *IEEE Transactions on Industrial Informatics*, 2023a.
- Yuanzhi Li, Sébastien Bubeck, Ronen Eldan, Allie Del Giorno, Suriya Gunasekar, and Yin Tat Lee. Textbooks are all you need ii: phi-1.5 technical report. *arXiv preprint arXiv:2309.05463*, 2023b.
- Yuhang Li, Ruihao Gong, Xu Tan, Yang Yang, Peng Hu, Qi Zhang, Fengwei Yu, Wei Wang, and Shi Gu. Brecq: Pushing the limit of post-training quantization by block reconstruction. *arXiv preprint arXiv:2102.05426*, 2021.
- Zhengyi Li, Cong Guo, Zhanda Zhu, Yangjie Zhou, Yuxian Qiu, Xiaotian Gao, Jingwen Leng, and Minyi Guo. Efficient activation quantization via adaptive rounding border for post-training quantization. *arXiv preprint arXiv:2208.11945*, 2022.
- Ji Lin, Jiaming Tang, Haotian Tang, Shang Yang, Xingyu Dang, and Song Han. Awq: Activation-aware weight quantization for llm compression and acceleration. *arXiv preprint arXiv:2306.00978*, 2023.
- Stephanie Lin, Jacob Hilton, and Owain Evans. Truthfulqa: Measuring how models mimic human falsehoods. *arXiv preprint arXiv:2109.07958*, 2021.
- Shih-Yang Liu, Zechun Liu, and Kwang-Ting Cheng. Oscillation-free quantization for low-bit vision transformers. *arXiv preprint arXiv:2302.02210*, 2023a.
- Zechun Liu, Barlas Oguz, Changsheng Zhao, Ernie Chang, Pierre Stock, Yashar Mehdad, Yangyang Shi, Raghuraman Krishnamoorthi, and Vikas Chandra. Llm-qat: Data-free quantization aware training for large language models. *arXiv preprint arXiv:2305.17888*, 2023b.

- Zhenhua Liu, Yunhe Wang, Kai Han, Wei Zhang, Siwei Ma, and Wen Gao. Post-training quantization for vision transformer. *Advances in Neural Information Processing Systems*, 34:28092–28103, 2021.
- Yu Mao, Weilan Wang, Hongchao Du, Nan Guan, and Chun Jason Xue. On the compressibility of quantized large language models. *arXiv preprint arXiv:2403.01384*, 2024.
- Mitchell Marcus, Beatrice Santorini, and Mary Ann Marcinkiewicz. Building a large annotated corpus of english: The penn treebank. 1993.
- Stephen Merity, Caiming Xiong, James Bradbury, and Richard Socher. Pointer sentinel mixture models. *arXiv preprint arXiv:1609.07843*, 2016.
- Todor Mihaylov, Peter Clark, Tushar Khot, and Ashish Sabharwal. Can a suit of armor conduct electricity? a new dataset for open book question answering. *arXiv preprint arXiv:1809.02789*, 2018.
- Markus Nagel, Mart van Baalen, Tijmen Blankevoort, and Max Welling. Data-free quantization through weight equalization and bias correction. In *Proceedings of the IEEE/CVF International Conference on Computer Vision*, pages 1325–1334, 2019.
- Markus Nagel, Rana Ali Amjad, Mart Van Baalen, Christos Louizos, and Tijmen Blankevoort. Up or down? adaptive rounding for post-training quantization. In *International Conference on Machine Learning*, pages 7197–7206. PMLR, 2020.
- OpenAI. Openai: Chatgpt, 2022. URL <https://openai.com/blog/chatgpt>.
- Denis Paperno, Germán Kruszewski, Angeliki Lazaridou, Quan Ngoc Pham, Raffaella Bernardi, Sandro Pezzelle, Marco Baroni, Gemma Boleda, and Raquel Fernández. The lambada dataset: Word prediction requiring a broad discourse context. *arXiv preprint arXiv:1606.06031*, 2016.
- Gunho Park, Baeseong Park, Se Jung Kwon, Byeongwook Kim, Youngjoo Lee, and Dongsoo Lee. nuqmm: Quantized matmul for efficient inference of large-scale generative language models. *arXiv preprint arXiv:2206.09557*, 2022.
- Colin Raffel, Noam Shazeer, Adam Roberts, Katherine Lee, Sharan Narang, Michael Matena, Yanqi Zhou, Wei Li, and Peter J Liu. Exploring the limits of transfer learning with a unified text-to-text transformer. *The Journal of Machine Learning Research*, 21(1):5485–5551, 2020.
- Mher Safaryan and Peter Richtárik. Stochastic sign descent methods: New algorithms and better theory. In *International Conference on Machine Learning*, pages 9224–9234. PMLR, 2021.
- Keisuke Sakaguchi, Ronan Le Bras, Chandra Bhagavatula, and Yejin Choi. Winogrande: An adversarial winograd schema challenge at scale. *Communications of the ACM*, 64(9):99–106, 2021.
- Wenqi Shao, Mengzhao Chen, Zhaoyang Zhang, Peng Xu, Lirui Zhao, Zhiqian Li, Kaipeng Zhang, Peng Gao, Yu Qiao, and Ping Luo. Omniquant: Omnidirectionally calibrated quantization for large language models. *arXiv preprint arXiv:2308.13137*, 2023.
- Hanlin Tang, Yifu Sun, Decheng Wu, Kai Liu, Jianchen Zhu, and Zhanhui Kang. Easyquant: An efficient data-free quantization algorithm for llms. *arXiv preprint arXiv:2403.02775*, 2024.
- Gemma Team, Thomas Mesnard, Cassidy Hardin, Robert Dadashi, Surya Bhupatiraju, Shreya Pathak, Laurent Sifre, Morgane Rivière, Mihir Sanjay Kale, Juliette Love, et al. Gemma: Open models based on gemini research and technology. *arXiv preprint arXiv:2403.08295*, 2024.
- Hugo Touvron, Thibaut Lavril, Gautier Izacard, Xavier Martinet, Marie-Anne Lachaux, Timothée Lacroix, Baptiste Rozière, Naman Goyal, Eric Hambro, Faisal Azhar, et al. Llama: Open and efficient foundation language models. *arXiv preprint arXiv:2302.13971*, 2023a.
- Hugo Touvron, Louis Martin, Kevin Stone, Peter Albert, Amjad Almahairi, Yasmine Babaei, Nikolay Bashlykov, Soumya Batra, Prajjwal Bhargava, Shruti Bhosale, et al. Llama 2: Open foundation and fine-tuned chat models. *arXiv preprint arXiv:2307.09288*, 2023b.

- Hugo Touvron, Louis Martin, Kevin Stone, Peter Albert, Amjad Almahairi, Yasmine Babaei, Nikolay Bashlykov, Soumya Batra, Prajjwal Bhargava, Shruti Bhosale, et al. Meta llama 3: The most capable openly available llm to date, April 2024. URL <https://ai.meta.com/blog/meta-llama-3/>.
- Albert Tseng, Jerry Chee, Qingyao Sun, Volodymyr Kuleshov, and Christopher De Sa. Quip#: Even better llm quantization with hadamard incoherence and lattice codebooks. *arXiv preprint arXiv:2402.04396*, 2024.
- Kuan Wang, Zhijian Liu, Yujun Lin, Ji Lin, and Song Han. Haq: Hardware-aware automated quantization with mixed precision. In *Proceedings of the IEEE/CVF conference on computer vision and pattern recognition*, pages 8612–8620, 2019.
- Xiuying Wei, Ruihao Gong, Yuhang Li, Xianglong Liu, and Fengwei Yu. Qdrop: randomly dropping quantization for extremely low-bit post-training quantization. *arXiv preprint arXiv:2203.05740*, 2022a.
- Xiuying Wei, Yunchen Zhang, Xiangguo Zhang, Ruihao Gong, Shanghang Zhang, Qi Zhang, Fengwei Yu, and Xianglong Liu. Outlier suppression: Pushing the limit of low-bit transformer language models. *Advances in Neural Information Processing Systems*, 35:17402–17414, 2022b.
- Xiuying Wei, Yunchen Zhang, Yuhang Li, Xiangguo Zhang, Ruihao Gong, Jinyang Guo, and Xianglong Liu. Outlier suppression+: Accurate quantization of large language models by equivalent and optimal shifting and scaling. *arXiv preprint arXiv:2304.09145*, 2023.
- Guangxuan Xiao, Ji Lin, Mickael Seznec, Julien Demouth, and Song Han. Smoothquant: Accurate and efficient post-training quantization for large language models. *arXiv preprint arXiv:2211.10438*, 2022.
- Guangxuan Xiao, Ji Lin, Mickael Seznec, Hao Wu, Julien Demouth, and Song Han. Smoothquant: Accurate and efficient post-training quantization for large language models. In *International Conference on Machine Learning*, pages 38087–38099. PMLR, 2023.
- Zhewei Yao, Zhen Dong, Zhangcheng Zheng, Amir Gholami, Jiali Yu, Eric Tan, Leyuan Wang, Qijing Huang, Yida Wang, Michael Mahoney, et al. Hawq-v3: Dyadic neural network quantization. In *International Conference on Machine Learning*, pages 11875–11886. PMLR, 2021.
- Zhewei Yao, Xiaoxia Wu, Cheng Li, Stephen Youn, and Yuxiong He. Zeroquant-v2: Exploring post-training quantization in llms from comprehensive study to low rank compensation. *arXiv:2303.08302*, 2023.
- Zhihang Yuan, Lin Niu, Jiawei Liu, Wenyu Liu, Xinggang Wang, Yuzhang Shang, Guangyu Sun, Qiang Wu, Jiayang Wu, and Bingzhe Wu. Rptq: Reorder-based post-training quantization for large language models. *arXiv preprint arXiv:2304.01089*, 2023.
- Edouard Yvinec, Arnaud Dapogny, and Kevin Bailly. Nupes: Non-uniform post-training quantization via power exponent search. *arXiv preprint arXiv:2308.05600*, 2023a.
- Edouard Yvinec, Arnaud Dapogny, Matthieu Cord, and Kevin Bailly. Spiq: Data-free per-channel static input quantization. In *Proceedings of the IEEE/CVF Winter Conference on Applications of Computer Vision*, pages 3869–3878, 2023b.
- Rowan Zellers, Ari Holtzman, Yonatan Bisk, Ali Farhadi, and Yejin Choi. Hellaswag: Can a machine really finish your sentence? *arXiv preprint arXiv:1905.07830*, 2019.
- Bohan Zhuang, Mingkui Tan, Jing Liu, Lingqiao Liu, Ian Reid, and Chunhua Shen. Effective training of convolutional neural networks with low-bitwidth weights and activations. *IEEE Transactions on Pattern Analysis and Machine Intelligence*, 44(10):6140–6152, 2021.

A Quantization Cost

Table 8 compares the quantization costs of different methods, with all measurements conducted on a single NVIDIA A100 GPU with 80GB of memory. We ensure each evaluation process exclusively occupies one GPU, but CPU and other resources may be shared among different processes due to limited resource. For SignRound, we disabled `low_gpu_mem_usage` in our implementation to achieve faster tuning, albeit with higher memory usage. Nevertheless, LLaMAV2-70B was still able to run on an A100 GPU with 80GB of memory. Although HQQ is exceptionally fast, our methods outperform others in terms of speed. Table 9 also compares the costs between FlexRound, Adaptive Round, and our method.

Table 8: Quantization cost in seconds at W4G-1 for LLaMA2. Align with the accuracy experiments, Omniquant 70b is tested with 128 calibration samples, while all the others are tested with 512 samples.

Model	GPTQ	AWQ	HQQ	Omniquant	Ours
LLaMAV2-7B	1821	1328	19	10255	1041
LLaMAV2-13B	3266	2630	30	18186	1918
LLaMAV2-70B	18517	13586	119	35694	9116

Table 9: Quantization Time (seconds) of Rounding Methods at W4G-1 with 200 steps for LLaMA V2 Models and Mistral-7B.

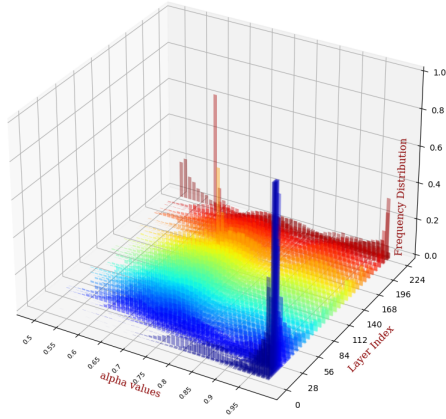
Method	FlexRound	AdaptiveRound	Ours
Mistral-7B-V0.1	9369	9332	1045
LLaMAV2-7B	9628	9701	1041
LLaMAV2-13B	17583	17865	1918

B View of distribution of tuned parameters

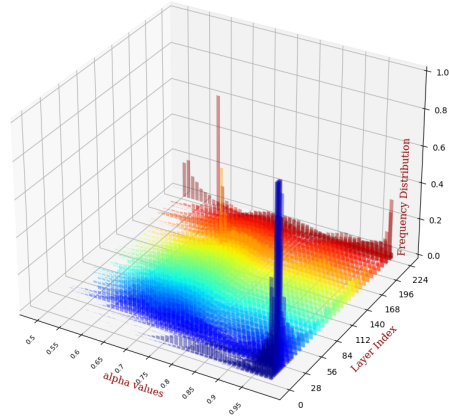
Figure 2 illustrates the distribution of the magnitudes of V in Eq.3 and α, β in Eq. 4 for Mistral-7B-v0.1 and LLaMA-2-7B at W4G-1. The results indicate that the distribution is flat for most layers, except for a few layers at the beginning and the end.

C Other results

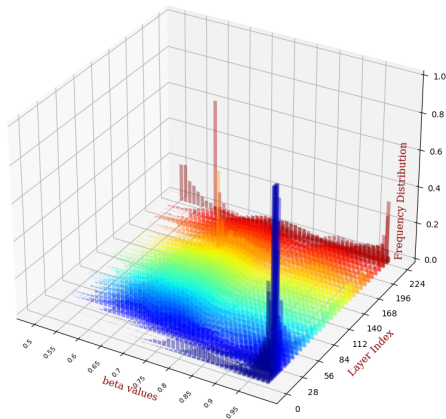
We present the detailed 11 tasks accuracy results for llama and mistral models with a size of 7-70B at W2-W4 in Table 10, 11, 12 and 13. the detailed PPL results in Table 14. Overall, our SignRound demonstrates a clear advantage in accuracy tasks, particularly in ultra-low bit quantization, achieving state-of-the-art performance compared to several popular weight quantization methods. In terms of perplexity (PPL), SignRound outperformed all other methods in 57 out of 112 scenarios, demonstrating its advantages. However, we observed that several quantization algorithms, including SignRound, exhibit sensitivity across different models and tasks. The reason for this sensitivity is detailed in Section 4.1.



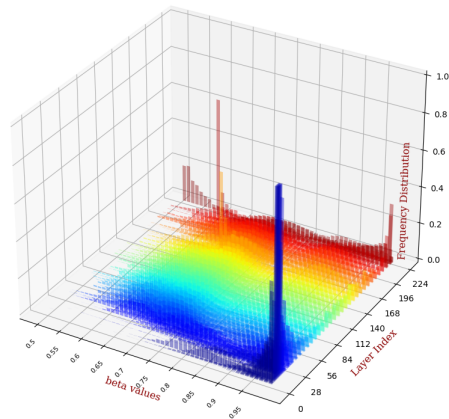
Mistral-7B, alpha values



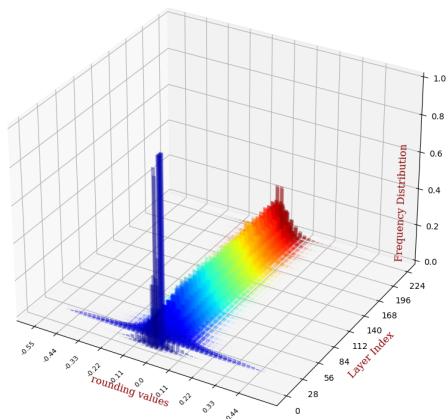
Llama-2-7B, alpha values



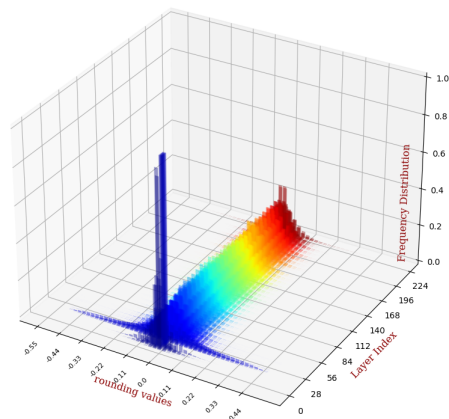
Mistral-7B, beta values



Llama-2-7B, beta values



Mistral-7B, V values



Llama-2-7B, V values

Figure 2: The distribution of the magnitude of V in Eq. 3 and α, β in Eq. 4 for Mistral-7B-v0.1 and LLaMA-2-7B at W4G-1, each color in the distribution represents a specific layer index in the models, with blue indicating shallow layers closer to the data layer, and red representing deeper layers.

Table 10: Accuracies(\uparrow) across 11 tasks(0-shot) of LLaMA and Mistral models at W4G-1. The notation GPTQ⁺ indicates that we adjusted the random seed or data pre-processing to address issues related to the non-positive definite Hessian matrix or other issues.

Model	Method	Mmlu	Lamb.	Hella.	Wino.	Piqa	Truth.	Open.	Boolq	RTE	ARC-e	ARC-c.	Avg.
V1-7B	FP16	32.74	73.53	56.94	70.01	78.67	22.03	34.60	75.08	66.43	75.25	41.81	57.01
	RTN	31.34	70.02	55.35	69.77	77.69	20.32	32.60	73.43	59.57	74.45	41.30	55.08
	GPTQ	29.06	71.08	55.11	70.01	77.37	20.93	32.20	72.69	63.90	74.66	41.64	55.33
	AWQ	33.33	70.81	55.98	68.27	78.07	21.18	31.40	74.37	64.62	74.03	41.21	55.75
	Omni	32.52	72.13	55.87	70.17	78.35	22.77	32.80	75.05	66.07	75.13	40.19	56.46
	Ours	31.80	71.96	56.57	69.53	79.00	21.91	33.20	75.72	66.79	74.83	43.09	56.76
V1-13B	FP16	44.21	76.21	59.92	72.77	79.16	25.70	33.20	77.89	70.76	77.40	46.42	60.33
	RTN	39.57	70.93	58.82	71.98	78.02	24.85	32.00	78.20	66.43	75.67	44.62	58.28
	GPTQ ⁺	40.01	74.67	58.92	71.03	78.45	26.44	33.60	77.09	68.23	76.85	44.97	59.12
	AWQ	44.56	74.13	59.13	71.27	78.94	25.83	33.20	76.42	66.06	76.89	46.67	59.37
	Omni	43.66	75.59	59.36	72.38	78.89	25.34	32.20	75.99	69.68	77.10	45.65	59.62
	Ours	43.94	75.82	59.51	72.22	78.78	25.70	32.80	77.34	67.51	76.47	46.67	59.71
V1-30B	FP16	55.14	77.55	63.33	75.85	81.12	28.27	36.00	82.78	66.79	80.39	52.90	63.65
	RTN	53.05	75.65	62.08	74.82	80.09	25.95	35.80	81.87	63.54	79.76	50.26	62.08
	GPTQ	53.04	77.22	61.95	73.80	80.69	27.29	34.60	81.07	66.06	78.79	49.15	62.15
	AWQ	54.13	76.77	62.78	74.11	81.07	27.78	35.00	82.66	67.15	79.97	51.71	63.01
	Omni	53.43	77.64	62.73	75.30	80.58	26.56	35.40	82.51	67.87	79.76	50.51	62.93
	Ours	54.72	77.84	62.91	75.06	80.69	26.68	36.40	82.60	66.79	80.13	52.13	63.27
V1-65B	FP16	59.79	79.12	64.53	77.35	81.23	27.91	38.00	84.86	69.68	81.36	52.82	65.15
	RTN	58.74	76.42	64.12	76.72	81.01	29.25	38.60	84.13	70.40	80.72	51.88	64.73
	GPTQ ⁺	59.10	78.17	63.78	75.69	81.34	28.27	38.40	83.76	68.59	80.98	51.62	64.52
	AWQ	58.86	77.37	63.86	76.56	80.85	28.27	35.20	83.94	71.48	78.75	50.94	64.19
	Omni	59.59	79.16	64.03	75.93	81.99	27.05	36.80	84.65	71.48	80.98	51.79	64.86
	Ours	59.21	79.16	64.37	76.64	81.34	26.81	37.80	84.40	69.68	80.98	51.79	64.74

Table 11: Accuracies(\uparrow) across 11 tasks(0-shot) of LLaMA and Mistral models at W4G128. The notation GPTQ⁺ indicates that we adjusted the random seed or data pre-processing to address issues related to the non-positive definite Hessian matrix or other issues.

Model	Method	Mmlu	Lamb.	Hella.	Wino.	Piqa	Truth.	Open.	Boolq	RTE	ARC-e	ARC-c.	Avg.
Mistral-7B	FP16	61.35	75.68	61.27	74.03	80.79	28.03	32.80	83.67	67.51	80.81	50.34	63.30
	RTN	59.72	74.44	61.06	73.40	80.36	27.17	32.60	83.67	64.62	79.63	49.32	62.36
	GPTQ	59.17	74.52	60.37	74.90	80.58	26.68	31.00	83.33	67.15	79.67	48.12	62.32
	AWQ	60.20	75.14	60.43	73.80	80.03	27.05	30.40	84.01	62.09	80.39	50.26	62.16
	HQQ	60.02	75.41	60.79	74.11	81.01	27.29	32.60	82.97	66.79	79.92	49.32	62.75
	Omni	59.71	73.94	60.62	73.56	80.36	26.68	30.80	83.58	65.70	80.01	49.06	62.18
	Ours	60.47	75.59	61.03	73.88	80.09	27.54	31.60	83.09	66.07	79.97	49.49	62.62
V2-7B	FP16	42.69	73.90	57.15	68.90	78.07	25.21	31.40	77.74	62.82	76.35	43.52	57.98
	RTN	40.91	72.44	56.91	68.35	77.58	24.97	31.20	77.61	56.32	76.26	43.52	56.92
	GPTQ	42.57	73.28	56.36	69.06	78.02	25.34	30.20	75.72	57.04	75.63	42.15	56.85
	AWQ	41.00	72.60	56.40	68.98	77.31	25.70	31.60	78.75	58.48	76.14	43.86	57.35
	HQQ	41.79	73.20	56.21	68.43	77.58	25.83	31.60	76.09	62.82	75.84	42.15	57.41
	Omni	41.72	73.04	56.59	68.98	77.91	24.97	30.80	75.81	61.37	75.76	43.34	57.30
	Ours	41.82	72.75	56.79	68.67	78.13	25.58	30.20	77.49	63.54	75.76	42.58	57.57
V2-13B	FP16	52.86	76.77	60.04	72.14	79.05	25.95	35.20	80.55	65.34	79.38	48.38	61.42
	RTN	52.10	76.27	59.77	72.14	78.62	24.72	34.20	80.24	62.09	79.00	47.95	60.65
	GPTQ	52.66	76.54	59.76	72.14	78.35	25.70	34.00	79.33	66.43	78.58	47.53	61.00
	AWQ	52.39	76.89	59.97	73.24	79.00	25.21	32.60	80.40	63.54	79.04	47.70	60.91
	HQQ	52.09	75.74	59.46	72.14	78.45	24.36	33.60	79.17	66.06	79.00	47.01	60.65
	Omni	52.01	76.17	59.53	72.06	78.35	23.87	33.40	80.80	66.07	78.37	47.18	60.51
	Ours	51.92	76.46	59.87	71.67	79.00	25.83	35.20	79.60	63.54	79.25	47.01	60.85
V2-70B	FP16	66.23	79.64	64.77	77.98	82.15	30.60	37.20	83.70	67.87	82.70	54.44	66.12
	RTN	64.91	79.06	63.93	78.14	81.66	30.11	37.00	83.61	68.59	82.79	54.78	65.87
	GPTQ	65.63	79.22	64.45	78.22	81.88	31.09	37.00	84.19	69.31	82.79	54.61	66.22
	AWQ	65.79	79.76	64.48	77.58	82.32	30.72	38.00	83.06	68.95	82.70	55.12	66.23
	HQQ	65.34	79.14	64.56	77.35	81.56	30.48	37.20	83.67	69.31	82.83	55.20	66.06
	Omni	65.30	79.39	64.52	77.51	81.88	30.60	37.40	83.39	68.23	82.91	55.12	66.02
	Ours	65.65	79.49	64.60	78.30	82.05	31.58	37.40	84.83	68.95	82.87	54.52	66.39
V1-7B	FP16	32.74	73.53	56.94	70.01	78.67	22.03	34.60	75.08	66.43	75.25	41.81	57.01
	RTN	32.63	72.31	56.26	70.01	78.45	20.93	33.60	74.74	64.26	74.71	42.75	56.42
	GPTQ	31.16	72.40	55.85	70.09	78.13	22.28	30.40	74.65	64.26	74.20	40.19	55.78
	AWQ	33.42	72.95	56.30	68.75	77.97	21.42	32.80	74.89	62.09	75.00	41.21	56.07
	Omni	31.15	72.35	56.25	69.22	78.35	21.42	33.80	74.74	65.70	74.87	42.06	56.36
	Ours	32.15	72.85	56.45	70.17	78.51	22.28	32.80	75.14	67.87	75.13	41.89	56.84
	V1-13B	FP16	44.21	76.21	59.92	72.77	79.16	25.70	33.20	77.89	70.76	77.40	46.42
RTN		42.71	75.26	59.30	72.53	79.54	25.95	32.60	76.76	65.34	76.98	45.82	59.34
GPTQ ⁺		42.65	75.41	59.51	72.93	79.33	24.97	32.40	77.49	68.23	76.89	45.56	59.58
AWQ		42.66	75.76	59.50	72.77	78.89	26.56	33.60	77.46	68.59	76.94	45.48	59.84
Omni		43.99	76.29	59.53	73.56	79.43	25.83	33.20	77.58	67.15	76.64	45.48	59.88
Ours		42.27	76.17	59.53	73.56	79.33	25.70	32.80	78.20	70.04	76.94	46.25	60.07
V1-30B		FP16	55.14	77.55	63.33	75.85	81.12	28.27	36.00	82.78	66.79	80.39	52.90
	RTN	54.24	77.02	62.90	74.35	80.52	27.29	34.20	81.96	67.15	80.89	52.05	62.96
	GPTQ	54.20	77.41	62.79	75.14	80.41	27.54	34.60	81.93	67.51	80.05	50.51	62.92
	AWQ	55.14	77.49	63.08	75.77	80.52	27.29	34.20	82.87	67.15	80.43	52.90	63.35
	Omni	55.22	77.80	63.09	75.14	80.30	28.52	36.00	82.20	69.31	80.81	52.82	63.75
	Ours	54.68	77.90	62.93	74.82	80.47	28.15	35.80	82.39	66.79	80.13	51.11	63.20
	V1-65B	FP16	59.79	79.12	64.53	77.35	81.23	27.91	38.00	84.86	69.68	81.36	52.82
RTN		59.53	79.51	64.63	77.35	80.96	27.91	38.40	84.43	71.48	81.48	52.22	65.26
GPTQ ⁺		60.47	78.79	64.45	76.24	81.18	28.03	37.40	83.85	68.95	81.57	53.07	64.91
AWQ		59.45	79.31	64.67	76.72	81.56	28.15	38.00	84.43	71.12	81.10	52.13	65.15
Omni		59.27	78.65	64.48	76.87	81.23	27.78	39.00	84.13	70.76	81.57	53.07	65.17
Ours		58.93	79.22	64.48	77.03	81.28	27.91	38.60	84.31	70.76	81.19	52.22	65.08

Table 12: Accuracies(\uparrow) across 11 tasks(0-shot) of LLaMA and Mistral models at W3G128. The notation GPTQ⁺ indicates that we adjusted the random seed or data pre-processing to address issues related to the non-positive definite Hessian matrix or other issues.

Model	Method	Mmlu	Lamb.	Hella.	Wino.	Piqa	Truth.	Open.	Boolq	RTE	ARC-e	ARC-c.	Avg.
Mistral-7B	FP16	61.35	75.68	61.27	74.03	80.79	28.03	32.80	83.67	67.51	80.81	50.34	63.30
	RTN	53.49	68.74	58.12	68.27	79.33	24.60	29.60	79.97	57.40	76.89	43.77	58.20
	GPTQ	55.84	73.04	57.61	70.24	78.67	24.85	30.80	81.44	63.54	77.27	45.65	59.91
	AWQ	55.61	73.69	57.86	71.27	79.82	26.07	29.00	81.10	59.21	79.00	46.93	59.96
	HQQ	53.97	68.66	58.59	72.22	78.73	25.70	30.00	80.24	63.90	76.81	43.86	59.33
	Omni	54.79	69.34	58.42	68.51	79.38	24.85	28.80	80.15	56.68	77.74	45.14	58.53
	Ours	57.54	73.01	59.60	72.85	79.54	25.70	31.60	81.74	58.12	78.70	46.33	60.43
V2-7B	FP16	42.69	73.90	57.15	68.90	78.07	25.21	31.40	77.74	62.82	76.35	43.52	57.98
	RTN	34.22	65.96	54.90	67.56	76.28	24.48	30.80	71.68	54.51	72.98	38.57	53.81
	GPTQ	36.11	69.61	53.66	68.59	76.01	21.91	27.80	73.43	54.51	73.74	40.19	54.14
	AWQ	35.82	69.90	54.98	67.40	76.01	25.21	29.80	74.68	57.76	74.07	41.64	55.21
	HQQ	34.40	66.64	53.27	67.01	75.46	25.46	28.80	73.58	61.37	72.94	38.48	54.31
	Omni	34.51	69.75	54.42	66.69	76.77	24.24	31.40	73.21	56.68	74.37	39.85	54.72
	Ours	40.13	71.01	55.33	68.27	76.82	25.34	32.80	75.32	60.29	75.25	42.92	56.68
V2-13B	FP16	52.86	76.77	60.04	72.14	79.05	25.95	35.20	80.55	65.34	79.38	48.38	61.42
	RTN	48.01	72.33	57.74	70.72	78.07	25.21	32.00	77.28	60.65	77.69	44.62	58.57
	GPTQ	49.56	75.24	57.83	70.88	78.56	24.97	33.40	78.44	62.82	77.99	45.65	59.58
	AWQ	49.77	75.22	58.58	71.82	77.75	24.11	34.20	79.97	53.43	77.95	44.62	58.86
	HQQ	48.40	73.22	57.66	69.77	77.31	24.11	30.60	76.97	60.29	77.15	43.60	58.10
	Omni	47.25	73.67	58.46	70.01	78.40	24.36	33.60	79.79	64.62	77.86	46.16	59.18
	Ours	49.64	75.20	59.11	71.59	78.29	24.85	34.20	78.47	58.12	78.58	45.82	59.44
V2-70B	FP16	66.23	79.64	64.77	77.98	82.15	30.60	37.20	83.70	67.87	82.70	54.44	66.12
	RTN	61.15	77.95	61.98	77.90	80.79	29.74	36.00	81.28	64.62	81.10	52.39	64.08
	GPTQ	63.15	79.06	62.94	77.66	81.45	30.72	36.20	81.53	67.87	81.65	53.67	65.08
	AWQ	64.09	79.47	63.75	76.48	81.77	29.74	37.20	82.69	66.06	81.40	53.67	65.12
	HQQ	63.45	78.05	63.12	77.03	81.01	29.38	36.60	82.23	66.43	81.78	53.67	64.80
	Omni	63.18	78.63	63.54	76.48	81.50	30.35	35.80	82.57	70.40	81.02	52.82	65.12
	Ours	64.94	78.89	63.83	76.56	81.50	31.21	37.20	81.41	68.59	81.73	52.56	65.31
V1-7B	FP16	32.74	73.53	56.94	70.01	78.67	22.03	34.60	75.08	66.43	75.25	41.81	57.01
	RTN	28.00	67.67	53.43	66.38	76.50	21.42	31.20	72.72	59.21	70.92	38.31	53.25
	GPTQ	30.16	66.31	53.92	67.48	76.82	21.42	29.60	71.31	59.21	72.22	38.74	53.38
	AWQ	30.33	70.19	54.53	68.98	76.71	20.81	31.60	74.68	64.62	73.23	38.91	54.96
	Omni	28.35	70.54	54.48	68.27	77.48	21.05	29.40	72.29	66.07	72.73	37.12	54.34
	Ours	25.85	70.95	55.45	69.69	77.37	21.66	32.00	73.88	60.29	73.48	39.33	54.54
	V1-13B	FP16	44.21	76.21	59.92	72.77	79.16	25.70	33.20	77.89	70.76	77.40	46.42
RTN		34.87	69.65	57.25	70.48	77.31	26.93	32.00	71.44	62.82	75.63	43.94	56.57
GPTQ		35.51	73.08	57.89	70.80	77.37	24.48	31.40	77.52	62.82	74.41	43.26	57.14
AWQ		40.53	73.94	57.89	69.53	78.94	26.68	33.40	74.83	65.34	75.93	45.05	58.37
Omni		38.35	74.42	57.79	70.80	78.07	26.68	33.20	75.81	65.34	75.88	43.69	58.18
Ours		39.16	75.22	58.64	71.59	78.94	25.95	35.20	76.30	65.34	76.52	45.39	58.93
V1-30B		FP16	55.14	77.55	63.33	75.85	81.12	28.27	36.00	82.78	66.79	80.39	52.90
	RTN	52.41	75.08	61.45	74.27	79.87	25.95	33.00	81.38	65.34	79.12	48.89	61.52
	GPTQ	51.39	74.97	60.35	75.30	79.60	26.93	34.80	82.75	64.62	78.11	48.46	61.57
	AWQ	53.84	76.71	61.94	75.14	80.03	25.34	34.40	81.90	67.15	79.59	50.77	62.44
	Omni	53.67	76.95	61.82	74.51	80.14	25.95	34.40	81.10	66.07	79.76	48.21	62.05
	Ours	54.39	77.49	62.13	74.03	80.47	27.30	35.00	79.76	68.59	79.46	48.98	62.51
	V1-65B	FP16	59.79	79.12	64.53	77.35	81.23	27.91	38.00	84.86	69.68	81.36	52.82
RTN		57.47	77.43	63.23	75.93	80.41	28.64	38.40	82.69	66.43	80.22	51.19	63.82
GPTQ ⁺		57.92	78.69	62.98	76.87	80.63	27.66	37.60	84.16	68.95	80.89	51.19	64.32
AWQ		58.87	77.94	63.77	75.37	80.96	27.66	36.80	85.02	71.12	81.10	50.34	64.45
Omni		57.19	77.00	63.15	75.53	80.90	28.15	37.60	83.18	69.68	80.18	50.51	63.92
Ours		58.30	78.11	63.60	76.56	80.85	29.50	37.80	84.80	70.04	80.22	50.68	64.59

Table 13: Accuracies(\uparrow) across 11 tasks(0-shot) of LLaMA and Mistral models at W2G128. The notation GPTQ⁺ indicates that we adjusted the random seed or data pre-processing to address issues related to the non-positive definite Hessian matrix or other issues.

Model	Method	Mmlu	Lamb.	Hella.	Wino.	Piqa	Truth.	Open.	Boolq	RTE	ARC-e	ARC-c.	Avg.
Mistral-7B	FP16	61.35	75.68	61.27	74.03	80.79	28.03	32.80	83.67	67.51	80.81	50.34	63.30
	RTN	23.45	0.14	27.43	49.64	54.30	24.24	15.20	38.69	51.99	29.08	21.59	30.52
	GPTQ	25.23	30.47	38.28	53.83	64.91	24.11	17.40	58.29	50.90	47.77	24.57	39.61
	AWQ	25.38	0.00	25.71	52.01	51.58	23.99	17.60	37.83	47.29	26.98	22.27	30.06
	HQQ	23.35	0.85	27.77	51.62	56.69	26.68	15.80	40.55	53.43	28.62	20.14	31.41
	Omni	23.24	5.38	29.38	49.72	56.09	26.32	16.60	41.99	52.71	32.11	20.39	32.17
	Ours	40.46	58.61	50.87	62.90	75.84	24.85	22.80	78.56	57.04	70.88	37.03	52.71
V2-7B	FP16	42.69	73.90	57.15	68.90	78.07	25.21	31.40	77.74	62.82	76.35	43.52	57.98
	RTN	23.98	0.02	26.04	49.49	52.50	24.85	15.20	41.01	49.10	27.48	19.71	29.94
	GPTQ	23.65	11.72	32.59	55.17	58.32	25.95	15.80	52.14	51.99	40.45	21.25	35.37
	AWQ	25.38	0.00	25.69	49.96	52.34	23.75	17.80	37.83	52.71	24.62	21.08	30.10
	HQQ	24.51	0.02	26.06	49.49	53.26	24.72	13.80	37.92	50.90	26.52	21.33	29.87
	Omni	22.97	35.53	40.28	55.88	65.13	22.89	15.60	63.24	53.07	50.13	23.46	40.74
	Ours	27.20	55.25	47.35	61.01	72.96	24.85	25.60	68.07	54.51	65.99	32.25	48.64
V2-13B	FP16	52.86	76.77	60.04	72.14	79.05	25.95	35.20	80.55	65.34	79.38	48.38	61.42
	RTN	23.77	7.47	33.08	49.01	57.94	26.19	16.00	47.74	53.43	32.03	21.93	33.51
	GPTQ	24.69	45.20	41.06	55.80	67.08	23.26	19.80	54.40	52.35	55.60	27.82	42.46
	AWQ	27.04	0.00	25.80	51.85	52.99	23.62	13.60	62.17	47.29	26.22	23.12	32.16
	HQQ	23.48	8.17	31.27	52.17	61.86	24.85	17.20	50.46	54.51	42.85	21.25	35.28
	Omni	25.53	49.84	46.23	57.93	70.13	24.60	21.80	66.85	55.60	63.22	30.29	46.55
	Ours	34.33	63.92	53.35	64.33	76.17	25.70	26.00	72.75	61.73	71.17	38.57	53.46
V2-70B	FP16	66.23	79.64	64.77	77.98	82.15	30.60	37.20	83.70	67.87	82.70	54.44	66.12
	RTN	24.20	20.18	40.88	54.85	63.87	24.11	17.60	43.06	53.07	50.51	27.22	38.14
	GPTQ	23.12	0.00	25.04	49.57	49.51	0.00	27.60	37.83	52.71	25.08	22.70	28.47
	AWQ	24.46	0.00	25.46	51.38	52.50	23.50	14.20	62.17	52.71	25.76	22.35	32.23
	HQQ	23.16	19.46	35.45	56.67	66.00	22.52	20.00	40.46	52.71	52.06	23.12	37.42
	Omni	33.84	61.83	52.44	64.33	74.10	24.48	28.20	71.68	53.07	67.21	33.28	51.31
	Ours	54.04	72.97	59.65	74.90	79.00	29.01	34.80	79.63	69.68	78.37	46.59	61.69
V1-7B	FP16	32.74	73.53	56.94	70.01	78.67	22.03	34.60	75.08	66.43	75.25	41.81	57.01
	RTN	24.36	0.52	27.24	49.25	54.24	24.24	15.20	39.63	57.40	27.86	21.84	31.07
	GPTQ	22.95	12.75	33.36	51.70	60.07	23.99	13.40	48.62	53.07	40.82	21.50	34.75
	AWQ	23.12	0.00	25.37	53.28	52.56	25.21	13.80	37.83	52.71	25.63	22.53	30.18
	Omni	23.58	44.23	42.39	58.48	68.82	21.54	20.40	60.80	53.07	59.55	27.56	43.68
	Ours	24.46	13.53	42.16	56.99	70.02	24.60	25.20	62.91	47.29	60.90	31.74	41.80
	V1-13B	FP16	44.21	76.21	59.92	72.77	79.16	25.70	33.20	77.89	70.76	77.40	46.42
RTN		24.66	4.97	29.67	49.33	57.24	25.58	12.40	44.10	53.79	32.07	22.01	32.35
GPTQ ⁺		26.43	40.48	39.47	58.25	66.97	23.50	18.60	52.78	50.54	51.52	25.00	41.23
AWQ		27.04	0.00	25.59	50.36	53.05	24.11	15.60	62.17	47.29	25.97	23.21	32.22
Omni		26.93	56.41	47.67	61.17	73.23	23.38	24.60	68.75	53.07	67.00	33.79	48.73
Ours		31.87	59.65	51.25	67.64	76.28	25.58	27.80	69.11	58.48	70.71	37.12	52.32
V1-30B		FP16	55.14	77.55	63.33	75.85	81.12	28.27	36.00	82.78	66.79	80.39	52.90
	RTN	23.24	5.55	27.22	53.99	56.80	21.79	18.20	51.65	53.07	36.74	21.33	33.60
	GPTQ	30.47	49.93	45.05	61.88	68.88	23.26	22.60	68.29	51.99	60.69	30.72	46.70
	AWQ	27.04	0.00	25.41	50.20	52.94	24.48	16.60	62.17	47.29	24.71	23.38	32.20
	Omni	26.89	63.03	52.23	64.64	74.27	23.87	29.20	70.86	54.51	70.45	36.18	51.47
	Ours	40.83	67.92	56.73	68.90	76.17	24.36	31.60	75.54	62.45	74.92	42.41	56.53
	V1-65B	FP16	59.79	79.12	64.53	77.35	81.23	27.91	38.00	84.86	69.68	81.36	52.82
RTN		24.48	32.78	43.59	57.85	67.52	22.89	22.80	61.53	50.54	52.10	28.24	42.21
GPTQ ⁺		37.06	67.44	53.97	69.46	76.44	24.36	28.00	73.64	60.29	71.34	38.57	54.60
AWQ		25.38	0.00	25.58	49.96	53.10	24.24	11.00	37.83	52.71	24.96	22.44	29.75
Omni		27.36	65.94	55.53	68.11	76.99	25.21	29.60	75.69	59.21	69.82	35.07	53.50
Ours		47.21	72.07	60.06	73.24	78.62	25.46	34.20	80.64	62.82	77.48	46.76	59.87

